



**Calhoun: The NPS Institutional Archive**  
**DSpace Repository**

---

NPS Scholarship

Publications

---

2015

# Surface and Airborne Measurements of Organosulfur and Methanesulfonate Over the Western United States and Coastal Areas

Sorooshian, Armin; Crosbie, Ewan; Maudlin, Lindsay C.;  
Youn, Jong-Sang; Wang, Zhen; Shingler, Taylor; Ortega,  
Amber M.; Hersey, Scott; Woods, Roy K.

---

Sorooshian, Armin, et al. "Surface and airborne measurements of organosulfur and methanesulfonate over the western United States and coastal areas." *Journal of Geophysical Research: Atmospheres*. v.120 no.16 (2015): pp. 8535-8548.  
<https://hdl.handle.net/10945/49690>

---

This publication is a work of the U.S. Government as defined in Title 17, United States Code, Section 101. Copyright protection is not available for this work in the

Downloaded from NPS Archive: Calhoun



Calhoun is the Naval Postgraduate School's public access digital repository for research materials and institutional publications created by the NPS community. Calhoun is named for Professor of Mathematics Guy K. Calhoun, NPS's first appointed -- and published -- scholarly author.

**Dudley Knox Library / Naval Postgraduate School**  
**411 Dyer Road / 1 University Circle**  
**Monterey, California USA 93943**

<http://www.nps.edu/library>



Published in final edited form as:

*J Geophys Res Atmos.* 2015 August 27; 120(16): 8535–8548. doi:10.1002/2015JD023822.

## Surface and Airborne Measurements of Organosulfur and Methanesulfonate Over the Western United States and Coastal Areas

Armin Sorooshian<sup>1,2,3,\*</sup>, Ewan Crosbie<sup>2</sup>, Lindsay C. Maudlin<sup>2</sup>, Jong-Sang Youn<sup>3</sup>, Zhen Wang<sup>1</sup>, Taylor Shingler<sup>1</sup>, Amber M. Ortega<sup>1</sup>, Scott Hersey<sup>4</sup>, and Roy K. Woods<sup>5</sup>

<sup>1</sup>Chemical and Environmental Engineering, University of Arizona, Tucson, AZ, United States

<sup>2</sup>Atmospheric Sciences, University of Arizona, Tucson, AZ, United States

<sup>3</sup>Mel and Enid Zuckerman College of Public Health, University of Arizona, Tucson, AZ, United States

<sup>4</sup>Olin College of Engineering, Needham, MA, United States

<sup>5</sup>Center for Interdisciplinary Remotely Piloted Aircraft Studies, Naval Postgraduate School, Monterey, CA, United States

### Abstract

This study reports on ambient measurements of organosulfur (OS) and methanesulfonate (MSA) over the western United States and coastal areas. Particulate OS levels are highest in summertime, and generally increase as a function of sulfate (a precursor) and sodium (a marine tracer) with peak levels at coastal sites. The ratio of OS to total sulfur (TS) is also highest at coastal sites, with increasing values as a function of Normalized Difference Vegetation Index (NDVI) and the ratio of organic carbon to elemental carbon. Correlative analysis points to significant relationships between OS and biogenic emissions from marine and continental sources, factors that coincide with secondary production, and vanadium due to a suspected catalytic role. A major OS species, methanesulfonate (MSA), was examined with intensive field measurements and the resulting data support the case for vanadium's catalytic influence. Mass size distributions reveal a dominant MSA peak between aerodynamic diameters of 0.32–0.56  $\mu\text{m}$  at a desert and coastal site with nearly all MSA mass (84%) in sub-micrometer sizes; MSA:non-sea salt sulfate ratios vary widely as a function of particle size and proximity to the ocean. Airborne data indicate that relative to the marine boundary layer, particulate MSA levels are enhanced in urban and agricultural areas, and also the free troposphere when impacted by biomass burning. Some combination of fires and marine-derived emissions leads to higher MSA levels than either source alone. Finally, MSA differences in cloud water and out-of-cloud aerosol are discussed.

---

\*Corresponding Author: Armin Sorooshian, armin@email.arizona.edu, Phone: (520) 626-5858, Fax: (520) 621-6048, Address: Department of Chemical and Environmental Engineering, University of Arizona, PO BOX 210011, Tucson, Arizona, 85721.

## 1. Introduction

Mounting evidence shows that organosulfur (OS) compounds are important components of ambient particulate matter [Gao et al., 2006; Surratt et al., 2007a; Gomez-Gonzalez et al., 2008; Lukacs et al., 2009; Russell et al., 2009; Chan et al., 2010; Claeys et al., 2010; Farmer et al., 2010; Froyd et al., 2010; Hawkins et al., 2010; Hatch et al., 2011a; b; Shakya and Peltier, 2013; Worton et al., 2013; Ma et al., 2014] and hydrometeors [Munger et al., 1986; Blando et al., 1998; Altieri et al., 2009; Mazzoleni et al., 2010; Pratt et al., 2013]. These species can potentially impact the hygroscopicity and surface tension of particles [Tao et al., 2014] and are useful tracers for secondary aerosol formation (SOA) [Liao et al., 2015]. Organosulfur precursors include sulfur dioxide (SO<sub>2</sub>) and volatile organic compounds (VOCs) originating from either biogenic [Betters and Hoffmann, 1987; Olson and Hoffmann, 1988; Liggio et al., 2005; Liggio and Li, 2006; Iinuma et al., 2007a, b; Froyd et al., 2010; Surratt et al., 2007b, 2008] or anthropogenic sources [Kundu et al., 2013; Ma et al., 2014; Staudt et al., 2014; Riva et al., 2015]. Marine sources include methanesulfonic acid formation from dimethylsulfide (DMS) emissions [Charlson et al., 1987] and oxidation of primary marine biomass [Claeys et al., 2010]. Organosulfur formation is reported to be affected by aerosol acidity [e.g., Surratt et al., 2007b; Liao et al., 2015], relative humidity [e.g., Perri et al., 2010; Zhang et al., 2011; McNeill et al., 2012; Huang et al., 2015; Liao et al., 2015], concentrations of nitrogen oxides (NO<sub>x</sub>) [e.g., Surratt et al., 2007a], and halogen chemistry [von Glasow and Crutzen, 2004].

Detection of individual OS compounds remains challenging with traditional techniques such as ion chromatography (IC). As a result, the difference between total sulfur (TS) and inorganic sulfur (IS) can be used to quantify the abundance of organosulfur (TS – IS = OS), which comprises organosulfates (R-O-SO<sub>3</sub><sup>-</sup>) and non-sulfate containing species such as methanesulfonate (MSA). This approach was used to estimate that OS compounds account for as much as 5–10% of organic mass in different regions of the United States [Tolocka and Turpin, 2012]. One of the more easily measured OS species is MSA, which is a major aerosol constituent in marine regions [e.g., Bates et al., 1992]. A utility of MSA data is that its ratio to non-sea salt (nss) sulfate has been used as a way of estimating the contribution of biogenic emissions to total sulfate [e.g., Gondwe et al., 2004 and references therein]. Of particular interest in this study is the potential role of vanadium in OS formation since it plays a catalytic role in the oxidation of DMS [Sahle-Demessie and Devulapelli, 2008] and S(IV) [Brandt and Vaneldik, 1995], and has been said to catalyze MSA formation in a previous field study in California [Gaston et al., 2010]; however, a complete understanding of the latter mechanism is lacking.

The goal of this work is to examine surface and airborne measurements of OS and MSA over the western United States and coastal areas, which cover a wide range of environmental conditions. The following questions are addressed: (i) how do OS concentrations and the OS:TS ratio vary spatiotemporally across the western United States and what factors are best correlated with their values?; (ii) how does the mass size distribution of MSA and its ratio to nss sulfate vary between a desert and coastal site?; (iii) what is the spatial distribution of MSA in particles and cloud water based on aircraft measurements?; and (iv) what factors are best correlated with MSA? The paper is organized as follows: (i) Section 2 describes

methods and datasets used; (ii) Section 3.1 presents surface aerosol data for OS and the OS:TS ratio in terms of spatiotemporal profiles and correlations with other factors across the western United States; (iii) Section 3.2 presents MSA data including surface aerosol mass size distribution data at a coastal and desert site (3.2.1), surface  $PM_{1.0}$  measurements at a desert site (3.2.2), and airborne  $PM_{1.0}$  and cloud water data over California, Oregon, and coastal areas (3.2.3); and (iv) Section 4 presents conclusions.

## 2. Experimental Methods

### 2.1 Organosulfur and Complementary Data

We utilize aerosol composition data from the EPA Interagency Monitoring of Protected Visual Environments (IMPROVE) network [Malm *et al.*, 1994; <http://views.cira.colostate.edu/fed/>]. IMPROVE aerosol monitoring stations are located primarily in National Parks and Wilderness Areas, collecting ambient aerosol on filters over a 24-h period every third day.  $PM_{2.5}$  samples are analyzed for ions, metals, organic carbon (OC) and elemental carbon (EC). Among the elemental measurements, x-ray fluorescence (XRF) is used for sulfur (S) and several other elements. Sampling protocols and additional details are provided elsewhere [[http://vista.cira.colostate.edu/improve/Publications/SOPs/UCDavis\\_SOPs/IMPROVE\\_SOPs.htm](http://vista.cira.colostate.edu/improve/Publications/SOPs/UCDavis_SOPs/IMPROVE_SOPs.htm)]. If the only difference between total and inorganic sulfur is due to measurement uncertainty (i.e., all TS is IS), then the TS:IS ratio would be normally distributed around 1.0; however, it has been shown that this is not the case and that median values of frequency distribution fits typically exceed unity across the United States, especially in our study region [Tolocka and Turpin, 2012]. This study uses data between 2005 and 2012 for stations shown in Figure 1a, with coordinates and altitudes shown in Table S1 (Supporting Information).

Temperature and precipitation data are obtained from the National Climatic Data Center (NCDC) for stations located close to each IMPROVE site for the period between 2005 and 2012 (site details in Table S1). Satellite data for relevant environmental parameters were obtained in pixels including the location of each IMPROVE site with specific spatial areas reported in Table S1. Data for cloud fraction, clear air Columnar Water Vapor (CWV), and Normalized Difference Vegetation Index (NDVI) were obtained from the Moderate Resolution Imaging Spectroradiometer (MODIS; Daily Level 3 data) [Remer *et al.*, 2005]. Here, NDVI is used as a proxy for biogenic emissions as has been done in a previous study in the southwestern United States [Youn *et al.*, 2013].

### 2.2 Methanesulfonate and Complementary Data

**2.2.1 Southern Arizona**—Aerosol and meteorological measurements were conducted from a rooftop laboratory on top of the Physics and Atmospheric Sciences Building on the University of Arizona campus in the urban center of Tucson, Arizona (32.23°N, 110.95°W); the site is referred to as the Tucson Aerosol Characterization Observatory (TACO). This site is ~25 km away from both the Saguaro National Monument and Saguaro West IMPROVE sites. Size-resolved aerosol composition was measured between 21 June—13 August 2013 using two Micro-Orifice Uniform Deposit Impactors [MOUDI, MSP Corporation; Marple *et al.*, 1991] with aerodynamic cut-point diameters of 0.056, 0.1, 0.18, 0.32, 0.56, 1.0, 1.8, 3.2,

5.6, 10.0, and 18.0  $\mu\text{m}$ . Teflon filters were used for MOUDI sampling (PTFE membrane, 2  $\mu\text{m}$  pore, 46.2 mm, Whatman). Sub-micrometer particular matter ( $\text{PM}_{1.0}$ ) composition between July 2012 and June 2013 was measured using a single-stage filter sampler (24–72 h) with pre-baked 47 mm quartz fiber filters (baking procedure details at <http://www.sunlab.com/sample-analysis/>). Extractions of filters were performed by using 10 mL of milli-Q water in sealed glass vials that were sonicated at 30 °C for 20 min. Samples were chemically analyzed with IC (Thermo Scientific Dionex ICS – 2100 system) and inductively coupled plasma mass spectrometry (ICP-MS; Agilent 7700 Series), details of which are reported elsewhere [Sorooshian et al., 2012].

**2.2.2 Oregon, California, and Coastal Areas**—The Nucleation in California Experiment (NiCE) was carried out with the Center for Interdisciplinary Remotely-Piloted Aircraft Studies (CIRPAS) Twin Otter between July and August 2013 over the northern half of California, southern Oregon, and coastal areas (total spatial area covered: 34°N—43°N, 119°W—126°W). MSA and other water-soluble species mass concentrations in  $\text{PM}_{1.0}$  were quantified with a particle-into-liquid sampler (PILS; Brechtel Mfg. Inc.) coupled to IC [Sorooshian et al., 2006]. Cloud water was collected using a modified Mohnen slotted-rod cloud water collector [Hegg and Hobbs, 1986], with specific details of the cloud water collection summarized elsewhere [Sorooshian et al., 2013a]. The same MOUDIs from TACO were deployed at a ground site during NiCE ~5 km from the coast in Marina, California (36.7°N, 121.8°W) to obtain size-resolved mass concentrations of MSA and other relevant species between 3 July and 9 August. Filter extracts and cloud water samples were chemically analyzed with the IC and ICP-MS techniques noted already. All sulfate data from TACO and NiCE correspond to non-sea salt (nss) sulfate with calculations relying on sodium measurements from the IC [i.e., sulfate:sodium is ~0.25 by weight for sea salt; Seinfeld and Pandis, 2012].

### 3. Results and Discussion

#### 3.1 IMPROVE Data Analysis

**3.1.1 Cluster Definitions and Spatial Distribution of OS and OS:TS**—The study region is divided into four clusters based on three factors: (i) geographic considerations; (ii) similar features associated with meteorology, geography, and NDVI (see spatial averages in Figure S1); and (iii) proximity of site-specific points to one another in the two-dimensional space comparing OS and OS:TS based on 8-year averaged data (see Figure 2). Cluster assignments for each site are shown in Table S1, with average OS mass concentration and OS:TS ratio of each site shown geographically in Figure 1b, and site-specific averages for parameters discussed below (OS, EC, sodium, sulfate, NDVI, OS:TS, OC:EC) in Table S2. Concentrations and ratios discussed in this sub-section are 8-year averages ( $\pm$  standard deviations).

The Coastal (“C”) cluster is defined by geographic considerations, as five sites are near coasts. This cluster exhibits the highest OS concentration ( $37 \pm 15 \text{ ng m}^{-3}$ ) and OS:TS ratio ( $0.15 \pm 0.02$ ). Inland California (“IC”) sites constitute another cluster and include a subset of sites in California with similar environmental characteristics such as NDVI. This cluster exhibits OS concentrations similar to the Coastal cluster ( $36 \pm 16 \text{ ng m}^{-3}$ ) and the third

highest OS:TS ratios ( $0.13 \pm 0.02$ ). Two pockets of data points emerge in Figure 2 that help define the other two clusters. Points with the lowest overall OS:TS ratios ( $0.10 \pm 0.02$ ) and among the narrowest range in OS concentrations ( $30 \pm 9 \text{ ng m}^{-3}$ ) constitute a Desert (“D”) cluster, while points for non-coastal sites with among the highest OS:TS ratios ( $0.15 \pm 0.02$ ) and lowest OS values ( $20 \pm 8 \text{ ng m}^{-3}$ ) form a North (“N”) cluster (i.e., northern part of study region).

Specific sites are labeled in Figure 2 that warrant discussion. The highest OS concentrations typically coincide with sites that have the highest concentrations of sulfate and sodium. Sulfate is a precursor to organosulfate production and sodium is representative of marine emissions owing to its association with sea salt. The lowest OS values ( $13\text{--}16 \text{ ng m}^{-3}$ ) are at high altitude sites (Hoover, Crater Lake, White Pass, Pasayten) exceeding 1600 m in elevation and removed from surface boundary layer ocean and urban emission sources. As compared to the “D” and “N” clusters, “C” and “IC” markers occupy a more expansive range of space in Figure 2, due to the broad intra-cluster range of both sulfate and sodium concentrations. In the “IC” cluster, the highest (lowest) OS concentrations are in Sequoia ( $65 \pm 29 \text{ ng m}^{-3}$ ) and Fresno ( $53 \pm 17 \text{ ng m}^{-3}$ ) (Hoover,  $16 \pm 8 \text{ ng m}^{-3}$ ), which exhibit the highest (lowest) sulfate and EC concentrations for that cluster (markers colored by sulfate in Figure 2). An intriguing result is that Sequoia exhibits a higher OS concentration than Fresno, which is influenced more strongly by urban emissions. This may be due to more secondary production of OS species in Sequoia, which exhibits a higher OC:EC ratio ( $6.41 \pm 1.06$  versus  $3.87 \pm 0.59$ ). This ratio is often used as a proxy for the strength of SOA formation versus direct carbonaceous aerosol emissions [Wolff *et al.*, 1981; Gray *et al.*, 1984; Turpin *et al.*, 1991].

In terms of the x-axis variability in Figure 2, a vertical bar denotes what is determined to be the study-region maximum value of the OS:TS ratio (0.17). This corresponds to the two coastal sites (Point Reyes and Redwood) with the least influence from anthropogenic pollution; these two sites have the lowest EC concentrations ( $0.06\text{--}0.08 \mu\text{g m}^{-3}$ ) and highest Na concentrations ( $0.40\text{--}0.84 \mu\text{g m}^{-3}$ ). Two factors helpful in explaining where markers are relative to this bar are NDVI (see marker sizes in Figure 2) and the OC:EC ratio. NDVI is highest in the “C” ( $0.69 \pm 0.02$ ) and “N” ( $0.53 \pm 0.02$ ) clusters and lowest in the “D” cluster ( $0.26 \pm 0.01$ ); NDVI is thought to be linked with biogenic emissions (e.g., Youn *et al.*, 2013), which can promote more formation of OS relative to IS, thus increasing the OS:TS ratio. Coastal points tend to shift to the left of the vertical bar as OC:EC ratios decrease, with the minimum being at Puget Sound (OC:EC =  $2.85 \pm 0.20$ ) due to significant anthropogenic influence; EC levels at Puget Sound are much higher ( $0.71 \pm 0.20 \mu\text{g m}^{-3}$ ) than the other “C” sites ( $0.05\text{--}0.15 \mu\text{g m}^{-3}$ ). The lowest overall OS:TS ratio was in Agua Tibia ( $0.09 \pm 0.02$ ), within the “D” cluster, coincident with some of the lowest OC:EC ratios ( $4.04 \pm 0.52$ ) and the highest sulfate concentrations ( $1.35 \pm 0.75 \mu\text{g m}^{-3}$ ), which reduces the OS:TS ratio value. The source of this sulfate is likely due to anthropogenic sources such as fossil fuel combustion, which is supported by one of the highest concentrations of the tracer species, vanadium ( $1.29 \pm 0.56 \text{ ng m}^{-3}$ ), among all sites examined. An outlier relative to other sites in the “D” cluster in Figure 2 is Death Valley with a higher OS:TS ratio ( $0.13 \pm 0.03$  versus

0.09—0.11 at other sites); this may be explained by this site having the highest intra-cluster OC:EC ratio ( $7.19 \pm 0.99$  versus 2.98—6.05 at other sites).

**3.1.2 Temporal Distribution of OS and OS:TS**—The monthly trend in cluster-averaged OS concentrations follows those of temperature and CWV with peaks between June and August and a minimum in the winter when cloud fraction is highest (Figure 3; individual sites shown in Figure S2). Previous work has also shown that OS species are abundant in warm summer months due to enhanced photooxidation processes [Tolocka and Turpin, 2012].

Higher OS:TS ratios are observed in wintertime (December–February) in the “IC” and “D” clusters, while comparable ratios are observed in the “C” and “N” clusters in both winters and summers (June–August) (Figure S2). As sulfate production is reduced in the winter relative to summer, the relative amount of OS to TS increases likely due to anthropogenic sources such as aromatic-derived VOC emissions [Kundu et al., 2013; Ma et al., 2014; Staudt et al., 2014; Riva et al., 2015] and biomass burning emissions [Shakya and Peltier, 2013]; the current dataset does not allow us to determine whether more volatilization of OS relative to IS in the summer helps explain higher OS:TS ratios in the winter. A plausible explanation for the comparable peak in OS:TS in the “C” and “N” clusters in the summer relative to winter may be due to more BVOC emissions (i.e., highest NDVI values in Table S2) than other clusters promoting OS formation rather than IS formation.

A second cloud fraction mode between July and August in the “D” cluster linked to the North American Monsoon does not result in any significant OS or OS:TS features that differ from other clusters with the exception perhaps of elevated sulfate production (thus driving down the OS:TS ratio) via aqueous processing (see peak CWV levels for “D” cluster in Figure 3). The annual profile of NDVI varies from other parameters in Figure 3, but as already noted, relative rankings of cluster-averaged values are similar to that of the OS:TS ratio. The next section more closely examines correlative relationships between OS, OS:TS, and other parameters.

**3.1.3 Interrelationships Across Study Region**—Table 1 summarizes significant correlations between OS and other parameters for the study region and individual clusters (refer to Tables S3–S7 for the complete correlation matrices between these parameters and also the OS:TS ratio). Monthly-averaged values of variables between 2005 and 2012 are used for this analysis, and only those correlations with statistical significance at 95% confidence using a two-tailed student’s t-test are reported. While the correlations do not prove causal relationships, they are useful for promoting additional investigation into potential relationships.

As expected from Figure 2, OS is best correlated with sulfate for the entire study region ( $r = 0.82$ ,  $n = 480$ ) and in each individual cluster ( $r = 0.85$ ) owing to their common precursor  $\text{SO}_2$ , as well as sulfate participating in formation of organosulfates [e.g., Liggio and Li, 2006]. Among meteorological variables, temperature and CWV exhibit the best correlation with OS ( $r = 0.59$ ) for the entire study region and individual clusters; these two parameters are coincident with photochemical and heterogeneous secondary aerosol formation [e.g.,

*Youn et al.*, 2013]. Both cloud fraction and precipitation are generally negatively correlated with OS ( $r = -0.44$ ) owing to OS being the lowest in the wintertime (Figure 3).

Sodium, vanadium, and potassium are positively correlated with OS in each cluster and the entire region. Sodium's highest correlation with OS is for the "C" cluster ( $r = 0.70$ ), which exhibits the widest intra-cluster range of values (Table S2). Sodium is a marine tracer and species co-emitted with it such as precursors to MSA and primary marine particles (e.g., sea salt) have OS constituents. While being associated with biomass burning emissions, potassium is also a component of sea salt, which may explain its significant correlation in all clusters. There are at least two potential explanations for the vanadium-OS correlation: (i) vanadium can play a catalytic role in the formation of OS via catalyzing MSA formation [*Gaston et al.*, 2010] or sulfate formation [e.g., *Ault et al.*, 2010], which could contribute to organosulfate production; and (ii) vanadium is emitted from shipping emissions along the western United States coast [e.g., *Wang et al.*, 2014], which is coincident with OS precursor emissions, such as  $\text{SO}_2$ . While the current dataset does not allow for quantification of the relative importance of these vanadium-related explanations in forming OS, it is worth noting that the correlation of vanadium with the OS:TS ratio is significantly negative across the entire region and all clusters except "N" (Tables S3–S7), which suggests that V, in its role as a tracer for  $\text{SO}_2$  or a catalyst, has a stronger role in helping to produce sulfate than OS.

The relationship between OS and ocean chlorophyll A, a proxy for phytoplankton biomass and often linked to high ocean biological productivity [e.g., *Andreae et al.*, 1994], was examined for the "C" cluster. MODIS AQUA data in adjacent  $1^\circ \times 1^\circ$  ocean areas to the west of Point Reyes, Redwood, and Kalmiopsis were used; the two sites in Washington (Olympic and Puget Sound) are omitted due to anthropogenic influence that can obfuscate the potential relationship between marine biological emissions and OS. The strongest correlation between chlorophyll A and any aerosol constituent was with sulfate ( $r = 0.59$ ; Table S4), which is followed by OS ( $r = 0.55$ ). This supports the notion that biogenic marine emissions are a significant contributor to OS formation [e.g., *Claeys et al.*, 2010; *Laing et al.*, 2013].

The complexity in OS formation is reflected in how a variety of major aerosol constituents (EC, OC, nitrate, silicon), stemming largely from anthropogenic, biomass burning, and soil emissions, do not consistently correlate with OS in individual clusters and only exhibit moderate to low coefficients for the entire study region ( $r \sim 0.19$ – $0.63$ ). NDVI exhibits a positive correlation only with the North cluster ( $r = 0.25$ ), albeit weak, probably due to it having the widest range of NDVI values of any cluster (Table S2).

Correlations between the OS:TS ratio and parameters in Table 1 are mostly opposite in sign to those for OS owing to the highest ratios generally being in the winter when most of these parameters exhibit minimum values (Tables S3–S7). The parameter exhibiting the strongest positive correlation with the OS:TS ratio across the entire study region is NDVI ( $r = 0.47$ ), as expected from Figure 2. This result is consistent with numerous recent reports of the influence of BVOC emissions on OS formation [e.g., *Liao et al.*, 2015 and references therein]. The IMPROVE-related parameter with the strongest correlation with the OS:TS ratio is the OC:EC ratio ( $r = 0.32$ ), with peak values of both being in the "C" and "N"

clusters (Table S2). The only cluster with a significant correlation between OS:TS and OC:EC was “C” ( $r = 0.47$ ) owing to the widest OC:EC range as Puget Sound is influenced strongly by anthropogenic pollution while Point Reyes and Redwood are the most pristine (based on EC values in Table S2).

The remainder of the study focuses on a specific OS species, MSA, to probe deeper into its character in the atmosphere, including its relationship with vanadium. While its mass concentration is only a fraction of OS, it is an important tracer species for marine emissions and it may have other undocumented sources that are explored below in continental areas.

## 3.2 Methanesulfonate

**3.2.1 Mass Size Distributions**—Mass size distribution data for MSA are informative about potential formation mechanisms [Lukacs *et al.*, 2009]. Data from Tucson (in spatial range of the “D” cluster) and Marina (in “C” cluster) reveal a dominant MSA peak between aerodynamic diameters of 0.32–0.56  $\mu\text{m}$ , similar to nss sulfate (Figure 4), with 84% (Tucson) and 95% (Marina) of MSA mass in the sub-micrometer size range. Between 70–90% of MSA was observed in the accumulation mode in the Finnish Arctic region with a similar mass size distribution [Kerminen *et al.*, 1997]. Total bulk MOUDI MSA concentrations, on average, were 101  $\text{ng m}^{-3}$  and 7  $\text{ng m}^{-3}$  in Marina and Tucson, respectively. Of the other elemental species examined in Table 1, vanadium most closely mimics the size distribution of MSA with a peak in the same size range, whereas the others have a peak in the coarse mode (K has peaks in both modes). Vanadium is elevated in concentration in the NiCE study region due to extensive shipping emissions [Coggon *et al.*, 2012; Wang *et al.*, 2014]. While similar mass size distributions cannot prove a catalytic relationship between vanadium and either MSA or nss sulfate (versus simply similar source profiles), the evidence at least supports the possibility.

The MSA:nss sulfate ratio has been characterized extensively in other regions [e.g., Gondwe *et al.*, 2004]; however, fewer data exist in terms of its size-resolved behavior, especially in a desert region. A higher ratio indicates that more of the nss sulfate mass burden is from DMS oxidation. Figure 4 shows that the ratio ranges from 0.01 to 0.11 in Marina, with values above 0.10 between 0.18–0.56  $\mu\text{m}$  and 1–1.8  $\mu\text{m}$ . Ratios in Tucson are expectedly lower and reach only as high as 0.02, and similar to Marina, the peak ratio is in the 1–1.8  $\mu\text{m}$  size range and lower values are observed at the smallest ( $< 0.1 \mu\text{m}$ ) and largest size ranges ( $> 5.6 \mu\text{m}$ ). These ratios are in the range of those reported in other global regions [Gondwe *et al.*, 2004]. However, in contrast to this study, size-resolved MSA:nss sulfate ratio data collected in the Finnish Arctic exhibited higher values in the Aitken mode ( $< 0.1 \mu\text{m}$ ) with lower values in the accumulation (0.3–0.5  $\mu\text{m}$ ) and super-micrometer modes [Kerminen *et al.*, 1997].

The Marina data indicate that the greatest DMS influence on nss sulfate is between 0.18–0.56  $\mu\text{m}$  due to gas-to-particle conversion processes (similar to nss sulfate) and between 1–1.8  $\mu\text{m}$  due to partitioning of gaseous MSA to coarse particle surfaces; the latter conclusion is supported by the mass size distribution of sodium (Figure 4a) revealing a super-micrometer mode consistent with the larger mode in the MSA:nss sulfate ratio. Only the larger mode is present in Tucson (Figure 4b), suggestive of particles in the 1–1.8  $\mu\text{m}$  range

being most successful to reach this desert site as a result of long-range transport; the mass size distribution of chloride (sodium not available) exhibits peak values where the MSA:nss sulfate ratio also is highest. A plausible sequence of events involves DMS vented to the free troposphere [Dibb *et al.*, 1999], leading to MSA that condenses on particles that eventually can be transported back to the boundary layer farther downwind [Jefferson *et al.*, 1998]; alternatively, marine aerosol containing MSA could be vented to the free troposphere and then transported. Figure 4 supports the conclusion of others [Kerminen *et al.*, 1997; Jefferson *et al.*, 1998] that the use of the MSA:nss sulfate ratio as a proxy for DMS oxidation influence on sulfate burden requires caution owing to the variation of this ratio across particle sizes and air mass type.

**3.2.2 PM<sub>1.0</sub> Interrelationships in the Desert Cluster**—As the previous MSA data discussed were during short-term field projects, PM<sub>1.0</sub> filter measurements collected year-round in Tucson are of interest to examine temporal trends of MSA and its relationships with other species (Table 2). Three seasons are examined: Pre-monsoon = May – June; Monsoon = July – September; Winter = November – January. The highest MSA concentrations occur in the Pre-monsoon season ( $9.5 \pm 5.2 \text{ ng m}^{-3}$ ), followed by the Monsoon ( $4.9 \pm 2.6 \text{ ng m}^{-3}$ ), and Winter ( $2.1 \pm 0.7 \text{ ng m}^{-3}$ ). Ratios of MSA:nss sulfate in these seasons were 0.008, 0.004, and 0.004, respectively. The seasonal MSA concentrations are correlated with influence from ocean emissions in Tucson as based on HYSPLIT back-trajectory analysis, with greater marine influence in Pre-monsoon months [Sorooshian *et al.*, 2013b].

Interestingly, MSA's highest correlation is with vanadium ( $r = 0.82$  for all seasons,  $r = 0.81$  for Pre-monsoon,  $r = 0.71$  for Monsoon). When an analogous correlation analysis as Table 2 is done for the MSA:nss sulfate ratio (Table S8), the strongest correlation is still with vanadium ( $r = 0.42$  for full year). This result is supportive of the previously mentioned catalytic role of vanadium in MSA formation. The next highest correlation between MSA and other aerosol constituents for the full year and the Pre-Monsoon and Monsoon seasons was with nss sulfate ( $r = 0.58$ ), consistent with common mass size distributions representative of a gas-to-particle formation mechanism. MSA exhibits insignificant correlations with other parameters in Winter due to its minimal concentrations and lack of variability. As residential wood burning is significant in the Winter in Tucson for organic aerosol formation [Youn *et al.*, 2013], the low MSA concentrations and lack of a correlation with oxalate (a biomass burning tracer) suggests that domestic burning is not a significant source for this species in southern Arizona.

**3.2.3 Airborne Measurements During NiCE**—To extend upon previously discussed surface observations of MSA and related species, airborne data of such species are now discussed to gain additional insight about (i) how MSA concentrations and the MSA:nss sulfate ratio vary for different air mass types, (ii) the vertical and spatial MSA concentration profiles in aerosol and cloud water, and (iii) interrelationships between MSA and other species. Due to the nature of the NiCE airborne measurements (i.e., fast time resolution on a moving platform), it was possible to isolate specific emissions sources as compared to the

previously discussed filter measurements that integrated data over much longer periods of time at a fixed location.

PILS measurements of  $PM_{1.0}$  were conducted over a broad region shown in Figure 5a that includes three of the clusters examined with IMPROVE data (“C”, “IC”, “N”). Table 3 categorizes measurements of MSA and MSA:nss sulfate in seven air mass categories: inland regions influenced by either (i) fires, (ii) urban pollution in Fresno, (iii) animal husbandry emissions from one of the largest cattle feedlots in the western United States [Sorooshian et al., 2008], or (iv) with no influence from any of the aforementioned sources (“background”); coastal areas (v) with and (vi) without influence from fires; and (vii) free tropospheric air. Inland and coastal areas are defined as being on the right or left, respectively, of the diagonal dashed line in Figure 5a. Criteria for designating airborne samples as having been influenced by biomass burning for the discussion below include visual and olfactory evidence, in addition to passive cavity aerosol spectrometer probe (PCASP;  $D_p \sim 0.1\text{--}2.6 \mu\text{m}$ ) number concentrations exceeding  $1000 \text{ cm}^{-3}$  [Prabhakar et al., 2014]. Oxalate concentrations are reported in Table 3 to quantify the influence of biomass burning in the study region [Prabhakar et al., 2014]. Oxalate’s average concentration was highest in the two fire categories, but its maximum concentration in the free troposphere ( $0.62 \mu\text{g m}^{-3}$ ) was comparable to that of the fire categories ( $0.40\text{--}0.73 \mu\text{g m}^{-3}$ ) owing to biomass burning plumes residing above the mixed layer.

The highest average MSA concentration ( $51 \pm 36 \text{ ng m}^{-3}$ ) coincides with the coastal fire category near the Redwood IMPROVE site. These samples were significantly impacted by the Big Windy and Whiskey Complex forest fires in southwest Oregon during NiCE [Coggon et al., 2014]. The background and fire-influenced inland categories exhibited the lowest average MSA levels ( $17 \pm 17 \text{ ng m}^{-3}$  and  $17 \pm 16 \text{ ng m}^{-3}$ , respectively). Since the coastal background category was similarly low in average MSA concentration ( $23 \pm 22 \text{ ng m}^{-3}$ ), one potential explanation for why the coastal fire category was enhanced in MSA is a synergistic interplay between biomass burning emissions (e.g., oxidants) and coastal emissions (e.g., DMS) that produces more MSA than either source alone. For example, NiCE MOUDI measurements indicate that vanadium levels during the period of biomass burning exceeded that of non-fire periods by more than a factor of two for the cumulative size distribution and also for size ranges relevant to the PILS and IMPROVE data; these enhanced concentrations could have promoted MSA production from its ocean-derived precursor emissions. But it is noted that the mass size distributions of MSA were nearly identical in fire and non-fire periods, with similar total mass concentrations, which could have been due to loss mechanisms during transport from the fires to the surface coastal site ( $\sim 47$  hours of transport time on average based on NOAA HYSPLIT back-trajectory analysis).

The second highest average MSA concentration ( $43 \pm 26 \text{ ng m}^{-3}$ ) was observed in Fresno where the effects of urban pollution are strongest among categories in Table 3. MSA has been linked to urban pollution in Beijing due to suspected DMS emissions from terrestrial emissions and dimethylsulphoxide from industrial waste [Yuan et al., 2004]. A cattle feedlot source is responsible for the third highest average concentration of MSA ( $35 \pm 23 \text{ ng m}^{-3}$ ), followed by the free troposphere ( $21 \pm 26 \text{ ng m}^{-3}$ ). However, the free troposphere exhibited

the highest maximum concentration ( $189 \text{ ng m}^{-3}$ ) and MSA:nss sulfate ratio (0.92), coincident with intercepted biomass burning plumes (Figure 5b). While these high values are due to biomass burning plumes, high ratios of MSA:nss sulfate aloft could also be due to a previously mentioned mechanism involving convective pumping of DMS from the boundary layer [Dibb et al., 1999], which can lead to MSA production. Past measurements in the region showed that an aerosol layer resides above cloud tops enriched with MSA that stem from free tropospheric transport [Sorooshian et al., 2007].

Figure 6 shows how the cloud water measurements of MSA compare to those from the PILS. MSA concentrations were much higher in cloud water (maximum =  $0.71 \text{ } \mu\text{g m}^{-3}$ ; average =  $0.21 \pm 0.17 \text{ } \mu\text{g m}^{-3}$ ) than in out-of-cloud  $\text{PM}_{1.0}$  due to the additional sources of super-micrometer particles containing MSA that activated into drops and dissolution of gaseous precursors such as DMS [e.g., Kerminen et al., 1997]. Cloud water ratios of MSA:nss sulfate generally exceed those from the PILS, with an average of  $0.27 \pm 0.18$  and maximum of 1.02. Higher ratios were generally observed between Redwood and Point Reyes (Figure 6a) where OS:TS ratios from IMPROVE were also highest as compared to all of the examined IMPROVE sites. The highest MSA concentrations and MSA:nss sulfate ratios were observed during periods of high sea salt (see markers colors in Figure 6b) and biomass burning influence; biomass burning impacted cloud water in the top portions of clouds due to entrainment during NiCE [Prabhakar et al., 2014]. A correlation analysis shows that cloud water MSA was best related to sea salt tracers (sodium and chloride:  $r = 0.56$ ,  $n = 119$ ) and nss sulfate ( $r = 0.66$ ,  $n = 91$ ); similar to the cloud water data, PILS MSA concentrations were best correlated with those of nss sulfate ( $r = 0.55$ ,  $n = 473$ ). The correlation of MSA with vanadium in cloud water was significant, although weak ( $r = 0.29$ ,  $n = 106$ ), while the vanadium-nss sulfate correlation was stronger at  $r = 0.65$  ( $n = 85$ ); these results are consistent with the IMPROVE data analysis, which supported vanadium as a tracer for  $\text{SO}_2$  and a catalyst for sulfate formation. Nonetheless, since MSA is expected to be a product of DMS oxidation, and is a non-sulfate containing OS species, the positive correlation between vanadium and MSA is still supportive of a catalytic role for vanadium in OS formation, distinct from any catalytic role it plays in sulfate formation.

#### 4. Conclusions

This work examined the nature of OS and MSA in diverse regions across the western United States and coastal areas using surface and airborne data. The main results are as follows following the order of issues raised at the end of Section 1:

- i. Analysis of EPA IMPROVE data shows that particulate OS levels are highest between June and August, and generally increase as a function of sulfate (a precursor) and sodium (a marine tracer) with peak levels at coastal sites. The ratio of OS to total sulfur (TS) is also highest at coastal sites and during the winter season except in regional clusters with elevated NDVI values that have comparable peaks in the summer presumably due to more BVOC emissions. Correlative analysis points to the importance of secondary production of OS species, continental and marine biogenic emissions, and a potential role for vanadium as a catalyst.

- ii. While bulk MSA concentrations were more than an order of magnitude higher at a Coastal site (Marina) versus a Desert site (Tucson), mass size distributions in both places reveal a dominant MSA peak between aerodynamic diameters of 0.32–0.56  $\mu\text{m}$ , similar to nss sulfate, with nearly all MSA mass (84%) being in the sub-micrometer size range. The MSA:nss sulfate ratio ranges from 0.01 to 0.11 in Marina, with peak values between 0.18–0.56  $\mu\text{m}$  and 1–1.8  $\mu\text{m}$ . Ratios in Tucson reach only as high as 0.02, and similar to Marina, the peak ratio is in the 1–1.8  $\mu\text{m}$  size range. These size ranges where peaks are observed are indicative of where biogenic influence on nss sulfate is most pronounced. The data indicate that particles in the 1–1.8  $\mu\text{m}$  size range are most successful to reach Tucson as a result of long-range transport of secondarily produced MSA.
- iii. Airborne measurements indicate the following: (i) enhanced MSA concentrations (the most during the NiCE campaign) are in the free troposphere coincident with biomass burning plumes; (ii) high MSA levels are observed in urban and feedlot areas; (iii) some combination of fires and marine-derived emissions leads to higher MSA levels than either source alone; and (iv) MSA levels and the MSA:nss sulfate ratio are much larger in cloud water than in  $\text{PM}_{1.0}$  due to some combination of super-micrometer particles containing MSA activating into drops and dissolution of gaseous precursors such as DMS.
- iv. Correlative analysis of year-long  $\text{PM}_{1.0}$  data in Tucson shows that MSA is most strongly related to vanadium due to a suspected catalytic effect. MSA was next best correlated with sulfate owing to a common gas-to-particle formation mechanism. NiCE aircraft measurements indicate that MSA is best related to marine tracers (e.g., sodium) and nss sulfate. While biomass burning resulted in enhanced MSA during NiCE, domestic burning in Tucson during the winter did not result in noticeable increases in MSA levels.

The results of this study build on the growing knowledge about the nature of OS and MSA in the ambient atmosphere. Of emerging importance in this and other studies is the complex interplay between anthropogenic and biogenic emissions in the life cycle of these species, including especially the impact of trace metals such as vanadium that warrants additional attention in subsequent studies. While other trace metals such as iron were not discussed in this study owing to their lower correlations with OS and MSA (in contrast to vanadium), they should be considered as well.

## Supplementary Material

Refer to Web version on PubMed Central for supplementary material.

## Acknowledgments

All data and results are available from the corresponding author (armin@email.arizona.edu). This research was supported in part by Grant 2 P42 ES04940–11 from the National Institute of Environmental Health Sciences (NIEHS) Superfund Research Program, NIH, and the Center for Environmentally Sustainable Mining through TRIF Water Sustainability Program funding at the University of Arizona. The measurements during NiCE were funded by ONR grants N00014-10-1-0200 and N00014-10-1-0811. Some of the analyses and visualizations used in this study were produced with the Giovanni online data system, developed and maintained by the NASA GES DISC.

We acknowledge the sponsors of the IMPROVE network and the Pima County Department of Environmental Quality for data. The authors acknowledge Hafliði Jonsson and Barbara Ervens for helpful discussions.

## References

- Altieri KE, Turpin BJ, Seitzinger SP. Oligomers, organosulfates, and nitrooxy organosulfates in rainwater identified by ultra-high resolution electrospray ionization FT-ICR mass spectrometry. *Atmos Chem Phys*. 2009; 9(7):2533–2542.
- Andreae TW, Andreae MO, Schebeske G. Biogenic sulfur emissions and aerosols over the tropical South-Atlantic. 1. Dimethylsulfide in seawater and in the atmospheric boundary-layer. *J Geophys Res*. 1994; 99(D11):22819–22829.
- Ault AP, Gaston CJ, Wang Y, Dominguez G, Thiemens MH, Prather KA. Characterization of the single particle mixing state of individual ship plume measured at the port of Los Angeles. *Environ Sci Technol*. 2010; 44(6):1954–1961. [PubMed: 20148582]
- Bates TS, Lamb BK, Guenther A, Dignon J, Stoiber RE. Sulfur emissions to the atmosphere from natural sources. *J Atmos Chem*. 1992; 14(1–4):315–337.
- Betterton EA, Hoffmann MR. Kinetics, mechanism, and thermodynamics of the reversible-reaction of methylglyoxal (CH<sub>3</sub>COCHO) with S(IV). *J Phys Chem US*. 1987; 91(11):3011–3020.
- Blando JD, Porcja RJ, Li TH, Bowman D, Lioy PJ, Turpin BJ. Secondary formation and the Smoky Mountain organic aerosol: An examination of aerosol polarity and functional group composition during SEAVS. *Environ Sci Technol*. 1998; 32(5):604–613.
- Brandt C, Vaneldik R. Transition-metal-catalyzed oxidation of sulfur(iv) oxides - atmospheric-relevant processes and mechanisms. *Chem Rev*. 1995; 95(1):119–190.
- Chan MN, et al. Characterization and quantification of isoprene-derived epoxydiols in ambient aerosol in the southeastern United States. *Environ Sci Technol*. 2010; 44(12):4590–4596. [PubMed: 20476767]
- Charlson RJ, Lovelock JE, Andreae MO, Warren SG. Oceanic phytoplankton, atmospheric sulfur, cloud albedo and climate. *Nature*. 1987; 326(6114):655–661.
- Claeys M, Wang W, Vermeylen R, Kourtev I, Chi XG, Farhat Y, Surratt JD, Gomez-Gonzalez Y, Sciare J, Maenhaut W. Chemical characterisation of marine aerosol at Amsterdam Island during the austral summer of 2006–2007. *J Aerosol Sci*. 2010; 41(1):13–22.
- Coggon MM, et al. Ship impacts on the marine atmosphere: insights into the contribution of shipping emissions to the properties of marine aerosol and clouds. *Atmos Chem Phys*. 2012; 12(18):8439–8458.
- Coggon MM, et al. Observations of continental biogenic impacts on marine aerosol and clouds off the coast of California. *J Geophys Res*. 2014; 119(11):6724–6748.
- Dibb JE, Talbot RW, Scheuer EM, Blake DR, Blake NJ, Gregory GL, Sachse GW, Thornton DC. Aerosol chemical composition and distribution during the Pacific Exploratory Mission (PEM) Tropics. *J Geophys Res*. 1999; 104(D5):5785–5800.
- Farmer DK, Matsunaga A, Docherty KS, Surratt JD, Seinfeld JH, Ziemann PJ, Jimenez JL. Response of an aerosol mass spectrometer to organonitrates and organosulfates and implications for atmospheric chemistry. *P Natl Acad Sci USA*. 2010; 107(15):6670–6675.
- Froyd KD, Murphy SM, Murphy DM, de Gouw JA, Eddingsaas NC, Wennberg PO. Contribution of isoprene-derived organosulfates to free tropospheric aerosol mass. *P Natl Acad Sci USA*. 2010; 107(50):21360–21365.
- Gao S, Surratt JD, Knipping EM, Edgerton ES, Shahgholi M, Seinfeld JH. Characterization of polar organic components in fine aerosols in the southeastern United States: Identity, origin, and evolution. *J Geophys Res*. 2006; 111(D14)
- Gaston CJ, Pratt KA, Qin XY, Prather KA. Real-time detection and mixing state of methanesulfonate in single particles at an inland urban location during a phytoplankton bloom. *Environ Sci Technol*. 2010; 44(5):1566–1572. [PubMed: 20121235]
- Gomez-Gonzalez Y, et al. Characterization of organosulfates from the photooxidation of isoprene and unsaturated fatty acids in ambient aerosol using liquid chromatography/(–) electrospray ionization mass spectrometry. *J Mass Spectrom*. 2008; 43(3):371–382. [PubMed: 17968849]

- Gondwe M, Krol M, Klaassen W, Gieskes W, de Baar H. Comparison of modeled versus measured MSA:nss SO<sub>4</sub> ratios: A global analysis. *Global Biogeochem Cy.* 2004; 18(2)
- Gray HA, Cass GR, Huntzicker JJ, Heyerdahl EK, Rau JA. Elemental and organic-carbon particle concentrations - a long-term perspective. *Sci Total Environ.* 1984; 36:17–25.
- Hatch LE, Creamean JM, Ault AP, Surratt JD, Chan MN, Seinfeld JH, Edgerton ES, Su YX, Prather KA. Measurements of isoprene-derived organosulfates in ambient aerosols by aerosol time-of-flight mass spectrometry - Part 1: Single particle atmospheric observations in Atlanta. *Environ Sci Technol.* 2011a; 45(12):5105–5111. [PubMed: 21604734]
- Hatch LE, Creamean JM, Ault AP, Surratt JD, Chan MN, Seinfeld JH, Edgerton ES, Su YX, Prather KA. Measurements of isoprene-derived organosulfates in ambient aerosols by aerosol time-of-flight mass spectrometry-Part 2: Temporal variability and formation mechanisms. *Environ Sci Technol.* 2011b; 45(20):8648–8655. [PubMed: 21905661]
- Hawkins LN, Russell LM, Covert DS, Quinn PK, Bates TS. Carboxylic acids, sulfates, and organosulfates in processed continental organic aerosol over the southeast Pacific Ocean during VOCALS-REx 2008. *J Geophys Res.* 2010; 115
- Hegg, DA.; Hobbs, PV. Second Annual Report on Project CAPA-21-80 to the Coordinating Research Council. 1986. Studies of the mechanisms and rate with which nitrogen species are incorporated into cloud water and precipitation.
- Huang DD, Li YJ, Lee BP, Chan CK. Analysis of Organic Sulfur Compounds in Atmospheric Aerosols at the HKUST Supersite in Hong Kong Using HR-ToF-AMS. *Environ Sci Technol.* 2015; 49(6):3672–3679. [PubMed: 25700022]
- Iinuma Y, Muller C, Boge O, Gnauk T, Herrmann H. The formation of organic sulfate esters in the limonene ozonolysis secondary organic aerosol (SOA) under acidic conditions. *Atmos Environ.* 2007a; 41(27):5571–5583.
- Iinuma Y, Muller C, Berndt T, Boge O, Claeys M, Herrmann H. Evidence for the existence of organosulfates from beta-pinene ozonolysis in ambient secondary organic aerosol. *Environ Sci Technol.* 2007b; 41(19):6678–6683. [PubMed: 17969680]
- Jefferson A, Tanner DJ, Eisele FL, Davis DD, Chen G, Crawford J, Huey JW, Torres AL, Berresheim H. OH photochemistry and methane sulfonic acid formation in the coastal Antarctic boundary layer. *J Geophys Res.* 1998; 103(D1):1647–1656.
- Kerminen VM, Aurela M, Hillamo RE, Virkkula A. Formation of particulate MSA: Deductions from size distribution measurements in the Finnish Arctic. *Tellus B.* 1997; 49(2):159–171.
- Kundu S, Quraishi TA, Yu G, Suarez C, Keutsch FN, Stone EA. Evidence and quantitation of aromatic organosulfates in ambient aerosols in Lahore, Pakistan. *Atmos Chem Phys.* 2013; 13(9):4865–4875.
- Laing JR, Hopke PK, Hopke EF, Husain L, Dutkiewicz VA, Paatero J, Viisanen Y. Long-term trends of biogenic sulfur aerosol and its relationship with sea surface temperature in Arctic Finland. *J Geophys Res.* 2013; 118(20)
- Liao J, et al. Airborne measurements of organosulfates over the continental US. *J Geophys Res.* 2015; 120(7):2990–3005.
- Liggio J, Li SM, McLaren R. Heterogeneous reactions of glyoxal on particulate matter: Identification of acetals and sulfate esters. *Environ Sci Technol.* 2005; 39(6):1532–1541. [PubMed: 15819206]
- Liggio J, Li SM. Organosulfate formation during the uptake of pinonaldehyde on acidic sulfate aerosols. *Geophys Res Lett.* 2006; 33(13)
- Lukacs H, Gelencser A, Hoffer A, Kiss G, Horvath K, Hartyani Z. Quantitative assessment of organosulfates in size-segregated rural fine aerosol. *Atmos Chem Phys.* 2009; 9(1):231–238.
- Ma Y, Xu XK, Song WH, Geng FH, Wang L. Seasonal and diurnal variations of particulate organosulfates in urban Shanghai, China. *Atmos Environ.* 2014; 85:152–160.
- Malm WC, Sisler JF, Huffman D, Eldred RA, Cahill TA. Spatial and Seasonal Trends in Particle Concentration and Optical Extinction in the United-States. *J Geophys Res.* 1994; 99(D1):1347–1370.
- Marple VA, Rubow KL, Behm SM. A Microorifice Uniform Deposit Impactor (Moudi) - Description, calibration, and use. *Aerosol Sci Tech.* 1991; 14(4):434–446.

- Mazzoleni LR, Ehrmann BM, Shen XH, Marshall AG, Collett JL. Water-soluble atmospheric organic matter in fog: Exact masses and chemical formula identification by ultrahigh-resolution fourier transform ion cyclotron resonance mass spectrometry. *Environ Sci Technol*. 2010; 44(10):3690–3697. [PubMed: 20397689]
- McNeill VF, Woo JL, Kim DD, Schwier AN, Wannell NJ, Sumner AJ, Barakat JM. Aqueous-phase secondary organic aerosol and organosulfate formation in atmospheric aerosols: A modeling study. *Environ Sci Technol*. 2012; 46(15):8075–8081. [PubMed: 22788757]
- Munger JW, Tiller C, Hoffmann MR. Identification of hydroxymethanesulfonate in fog water. *Science*. 1986; 231(4735):247–249. [PubMed: 17769644]
- Olson TM, Hoffmann MR. Formation kinetics, mechanism, and thermodynamics of glyoxylic acid-S(IV) adducts. *J Phys Chem US*. 1988; 92(14):4246–4253.
- Perri MJ, Lim YB, Seitzinger SP, Turpin BJ. Organosulfates from glycolaldehyde in aqueous aerosols and clouds: Laboratory studies. *Atmos Environ*. 2010; 44(21–22):2658–2664.
- Prabhakar G, et al. Sources of nitrate in stratocumulus cloud water: Airborne measurements during the 2011 E-PEACE and 2013 NiCE studies. *Atmos Environ*. 2014; 97:166–173.
- Pratt KA, Fiddler MN, Shepson PB, Carlton AG, Surratt JD. Organosulfates in cloud water above the Ozarks' isoprene source region. *Atmos Environ*. 2013; 77:231–238.
- Remer LA, et al. The MODIS aerosol algorithm, products, and validation. *J Atmos Sci*. 2005; 62(4): 947–973.
- Riva M, Tomaz S, Cui TQ, Lin YH, Perraudin E, Gold A, Stone EA, Villenave E, Surratt JD. Evidence for an unrecognized secondary anthropogenic source of organosulfates and sulfonates: gas-phase oxidation of polycyclic aromatic hydrocarbons in the presence of sulfate aerosol. *Environ Sci Technol*. 2015; 49(11):6654–6664. [PubMed: 25879928]
- Russell LM, Takahama S, Liu S, Hawkins LN, Covert DS, Quinn PK, Bates TS. Oxygenated fraction and mass of organic aerosol from direct emission and atmospheric processing measured on the R/V Ronald Brown during TEXAQS/GoMACCS 2006. *J Geophys Res*. 2009; 114
- Sahle-Deemessie E V, Devulapelli G. Vapor phase oxidation of dimethyl sulfide with ozone over V<sub>2</sub>O<sub>5</sub>/TiO<sub>2</sub> catalyst. *Appl Catal B-Environ*. 2008; 84(3–4):408–419.
- Seinfeld, JH.; Pandis, SN. *Atmospheric Chemistry and Physics: from Air Pollution to Climate Change*. John Wiley & Sons; 2012.
- Shakya KM, Peltier RE. Investigating missing sources of sulfur at Fairbanks, Alaska. *Environ Sci Technol*. 2013; 47(16):9332–9338. [PubMed: 23927829]
- Sorooshian A, Brechtel FJ, Ma YL, Weber RJ, Corless A, Flagan RC, Seinfeld JH. Modeling and characterization of a particle-into-liquid sampler (PILS). *Aerosol Sci Tech*. 2006; 40(6):396–409.
- Sorooshian A, Lu ML, Brechtel FJ, Jonsson H, Feingold G, Flagan RC, Seinfeld JH. On the source of organic acid aerosol layers above clouds. *Environ Sci Technol*. 2007; 41(13):4647–4654. [PubMed: 17695910]
- Sorooshian A, Murphy SN, Hersey S, Gates H, Padro LT, Nenes A, Brechtel FJ, Jonsson H, Flagan RC, Seinfeld JH. Comprehensive airborne characterization of aerosol from a major bovine source. *Atmos Chem Phys*. 2008; 8(17):5489–5520.
- Sorooshian A, Csavina J, Shingler T, Dey S, Brechtel FJ, Saez AE, Betterton EA. Hygroscopic and chemical properties of aerosols collected near a copper smelter: Implications for public and environmental health. *Environ Sci Technol*. 2012; 46(17):9473–9480. [PubMed: 22852879]
- Sorooshian A, Wang Z, Coggon MM, Jonsson HH, Ervens B. Observations of sharp oxalate reductions in stratocumulus clouds at variable altitudes: Organic acid and metal measurements during the 2011 E-PEACE campaign. *Environ Sci Technol*. 2013a; 47(14):7747–7756. [PubMed: 23786214]
- Sorooshian A, Shingler T, Harpold A, Feagles CW, Meixner T, Brooks PD. Aerosol and precipitation chemistry in the southwestern United States: spatiotemporal trends and interrelationships. *Atmos Chem Phys*. 2013b; 13(15):7361–7379. [PubMed: 24432030]
- Staudt S, et al. Aromatic organosulfates in atmospheric aerosols: Synthesis, characterization, and abundance. *Atmos Environ*. 2014; 94:366–373.
- Surratt JD, et al. Evidence for organosulfates in secondary organic aerosol. *Environ Sci Technol*. 2007a; 41(2):517–527. [PubMed: 17310716]

- Surratt JD, Lewandowski M, Offenberg JH, Jaoui M, Kleindienst TE, Edney EO, Seinfeld JH. Effect of acidity on secondary organic aerosol formation from isoprene. *Environ Sci Technol.* 2007b; 41(15):5363–5369. [PubMed: 17822103]
- Surratt JD, et al. Organosulfate formation in biogenic secondary organic aerosol. *J Phys Chem A.* 2008; 112(36):8345–8378. [PubMed: 18710205]
- Tao S, Lu X, Levac N, Bateman AP, Nguyen TB, Bones DL, Nizkorodov SA, Laskin J, Laskin A, Yang X. Molecular characterization of organosulfates in organic aerosols from Shanghai and Los Angeles urban areas by nanospray-desorption electrospray ionization high-resolution mass spectrometry. *Environ Sci Technol.* 2014; 48(18):10993–11001. [PubMed: 25184338]
- Tolocka MP, Turpin B. Contribution of organosulfur compounds to organic aerosol mass. *Environ Sci Technol.* 2012; 46(15):7978–7983. [PubMed: 22731120]
- Turpin BJ, Huntzicker JJ, Larson SM, Cass GR. Los-Angeles summer midday particulate carbon - primary and secondary aerosol. *Environ Sci Technol.* 1991; 25(10):1788–1793.
- von Glasow R, Crutzen PJ. Model study of multiphase DMS oxidation with a focus on halogens. *Atmos Chem Phys.* 2004; 4:589–608.
- Wang Z, Sorooshian A, Prabhakar G, Coggon MM, Jonsson HH. Impact of emissions from shipping, land, and the ocean on stratocumulus cloud water elemental composition during the 2011 E-PEACE field campaign. *Atmos Environ.* 2014; 89:570–580.
- Wolff GT, Countess RJ, Groblicki PJ, Ferman MA, Cadle SH, Muhlbaier JL. Visibility-reducing species in the Denver “brown cloud”. 2. Sources and temporal patterns. *Atmos Environ.* 1981; 15(12):2485–2502.
- Worton DR, et al. Observational insights into aerosol formation from isoprene. *Environ Sci Technol.* 2013; 47(20):11403–11413. [PubMed: 24004194]
- Youn JS, et al. Evidence of aqueous secondary organic aerosol formation from biogenic emissions in the North American Sonoran Desert. *Geophys Res Lett.* 2013; 40(13):3468–3472. [PubMed: 24115805]
- Yuan H, Wang Y, Zhuang GS. MSA in Beijing aerosol. *Chinese Sci Bull.* 2004; 49(10):1020–1025.
- Zhang H, Surratt JD, Lin YH, Bapat J, Kamens RM. Effect of relative humidity on SOA formation from isoprene/NO photooxidation: enhancement of 2-methylglyceric acid and its corresponding oligoesters under dry conditions. *Atmos Chem Phys.* 2011; 11(13):6411–6424.

**Key Points**

1. Organosulfur (OS) and methanesulfonate (MSA) studied across western US in aerosol and cloud water
2. Vanadium positively related with OS and MSA due to presumed catalytic effect
3. MSA levels are enhanced in urban areas and when biomass burning and marine emissions interact

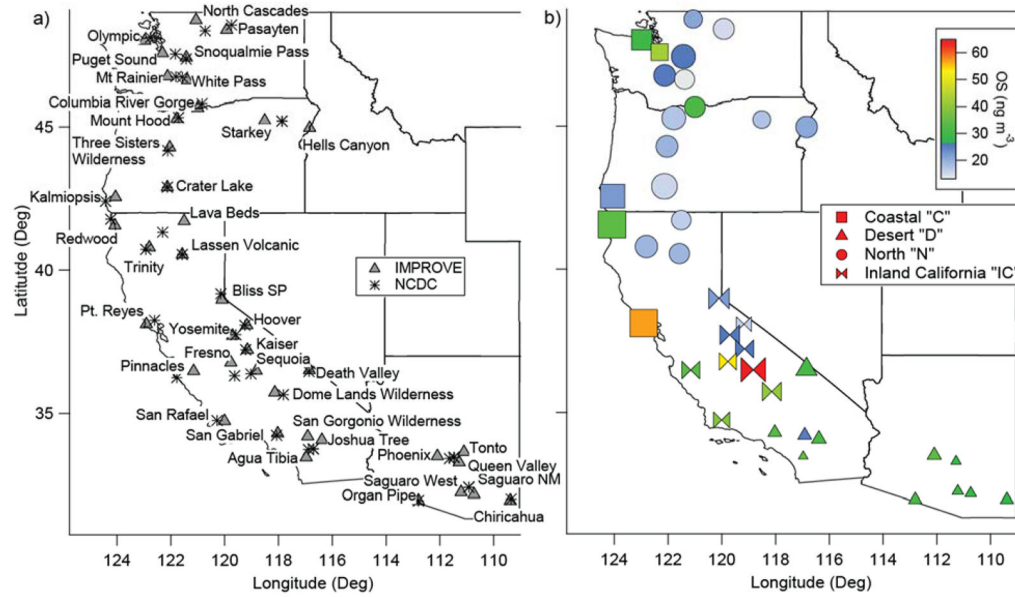


**Figure 1.**

(a) EPA IMPROVE (aerosol) and NCDC (meteorology) sites. (b) Average OS mass concentration at each IMPROVE site between 2005–2012. Marker size is proportional to OS:TS ratio (range: 0.09 – 0.17), and colored by OS mass concentration. Marker shape indicates cluster assignment.

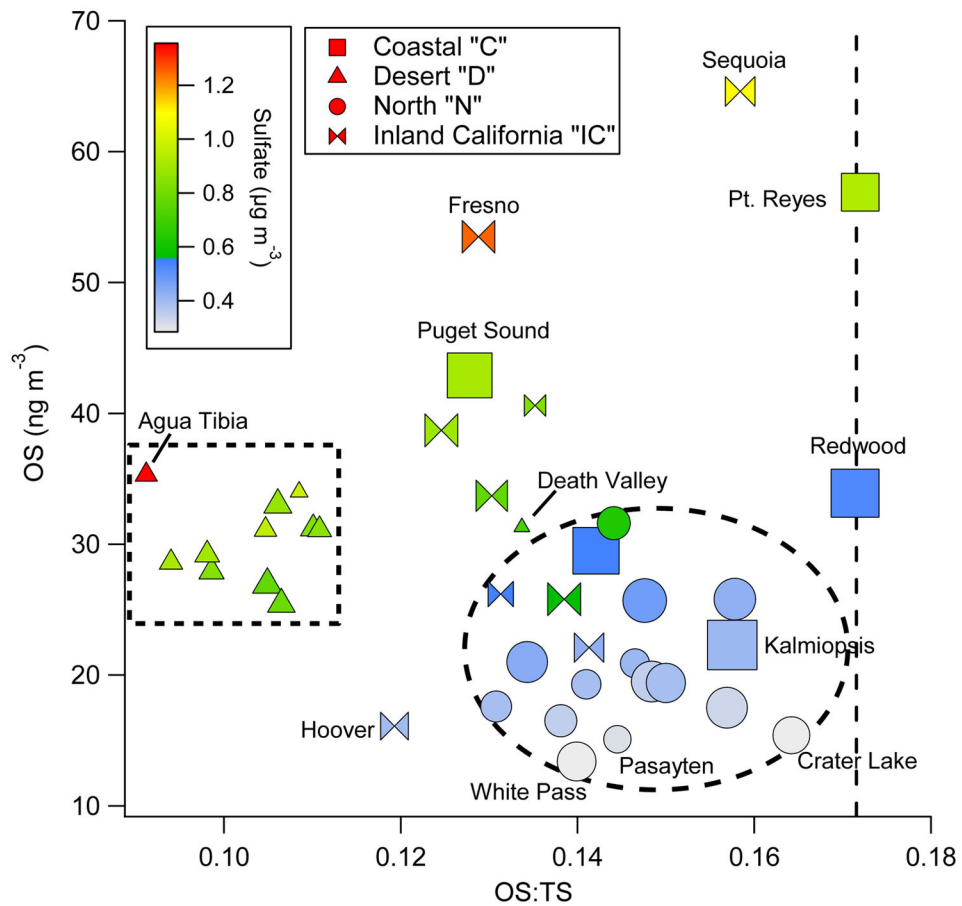


**Figure 2.** Scatterplot of 8-year averaged OS versus OS:TS for all IMPROVE sites in Figure 1. Marker sizes are proportional to NDVI (range = 0.13–0.76). Marker shapes correspond to assigned clusters for specific sites, with dashed enclosures representing “D” (square) and “N” (ellipse) clusters. The dashed vertical line on the right represents a OS:TS maximum value reflective of sites with the most marine influence and least affected by anthropogenic pollution. Specific sites of interest are labeled that are discussed.

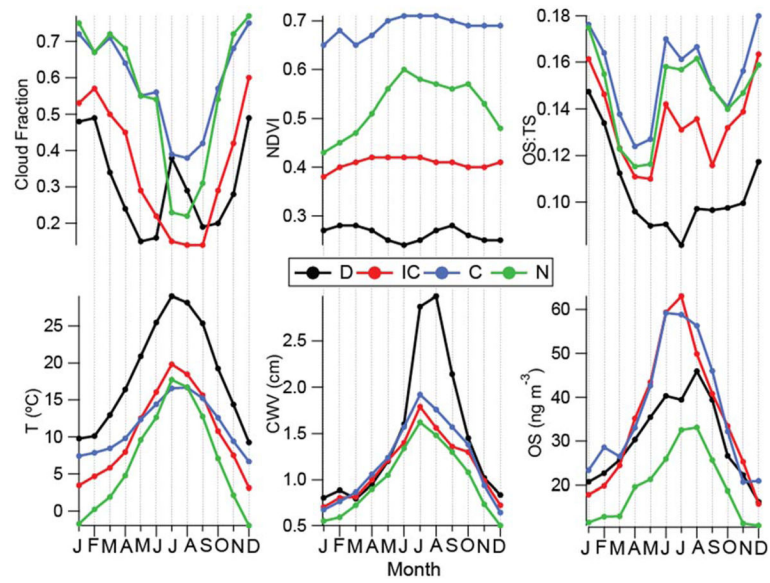


**Figure 3.** Monthly averages of environmental parameters (cloud fraction, Normalized Difference Vegetation Index, temperature, Columnar Water Vapor), OS:TS ratio, and OS mass concentration for sub-regional clusters for data between 2005–2012.

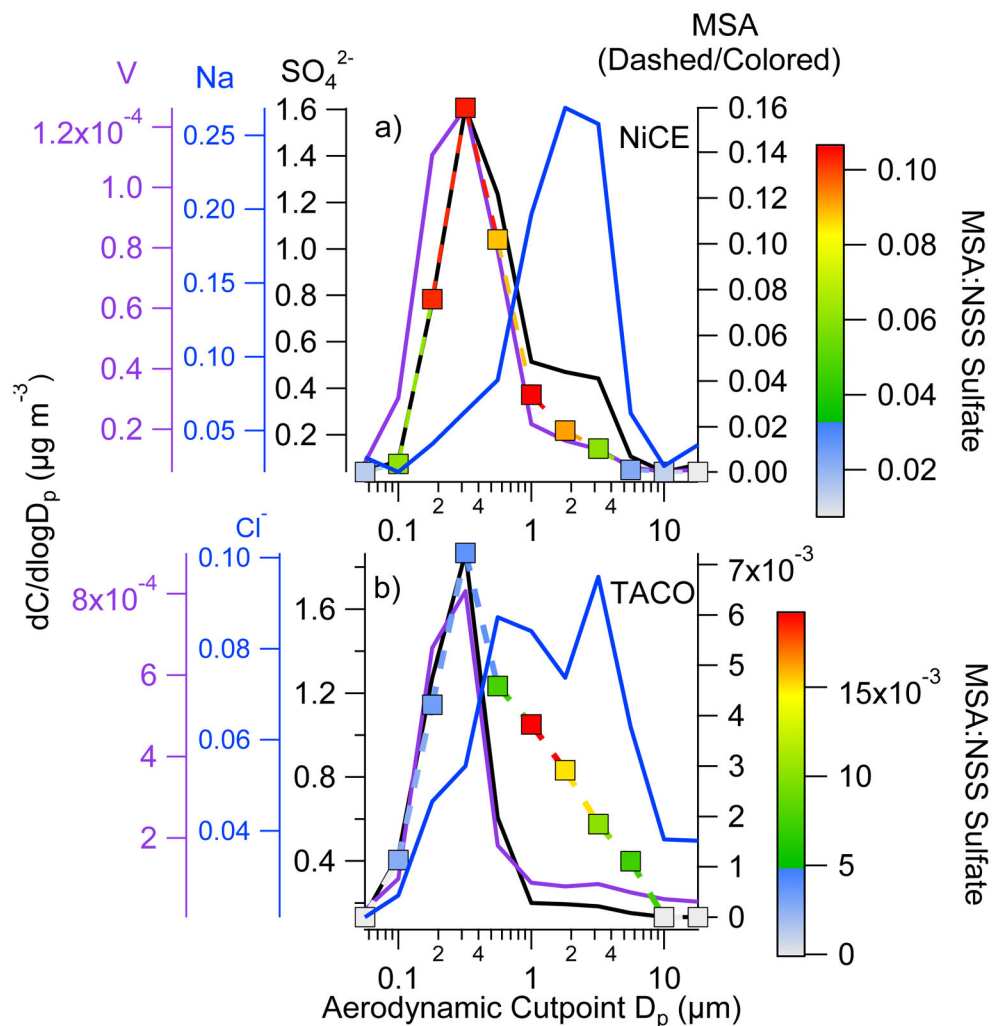


**Figure 4.** Size-resolved MOUDI measurements of MSA, vanadium, sodium, chloride, and nss sulfate concentration at the (a) Marina, California coastal site (NiCE) and the (b) Tucson, Arizona desert site (TACO).

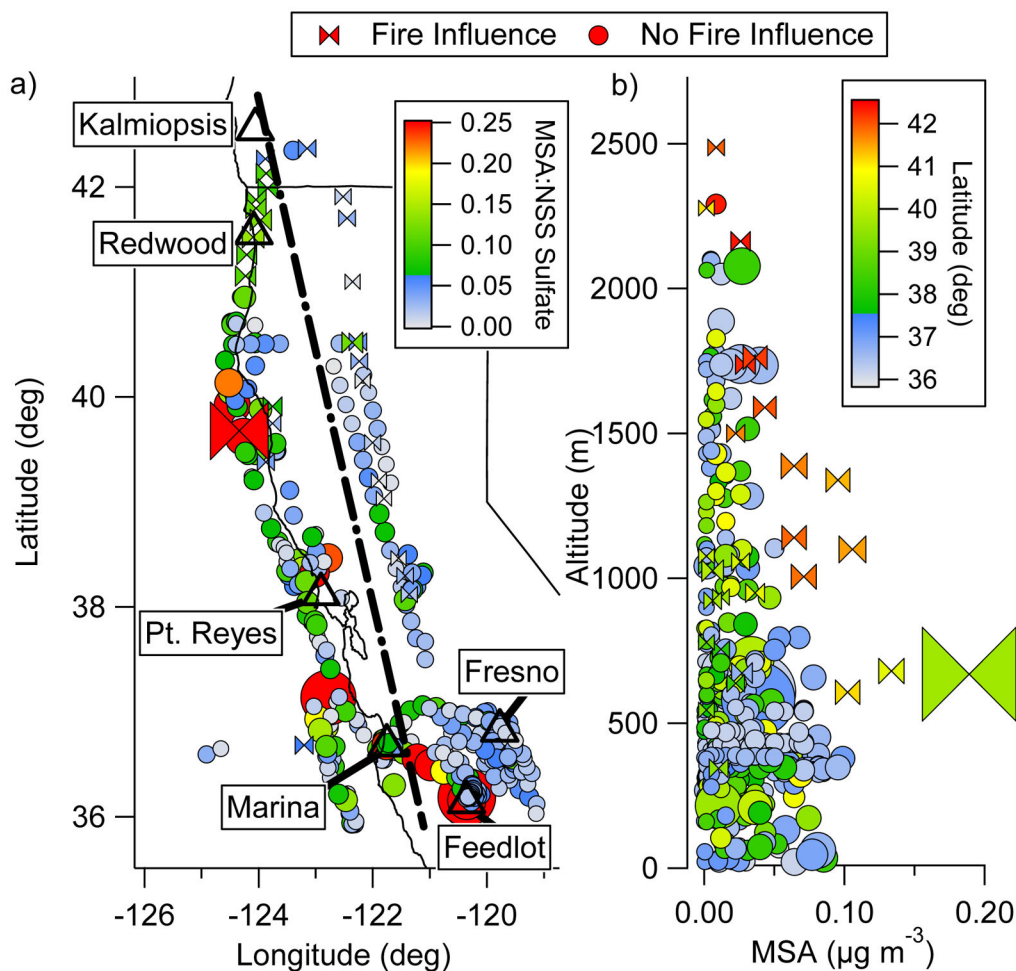


**Figure 5.**

(a) Spatial map of MSA in  $PM_{1.0}$  as measured by the CIRPAS Twin Otter during the NiCE campaign between July and August 2013. The dashed line divides the regions being examined in Table 3. Markers are sized by the MSA:nss sulfate ratio, which reaches as high as 0.92; the range is reduced on the color bar to highlight coastal and inland differences better. (b) Vertical profile of MSA concentration with marker size proportional to the MSA:nss sulfate ratio.

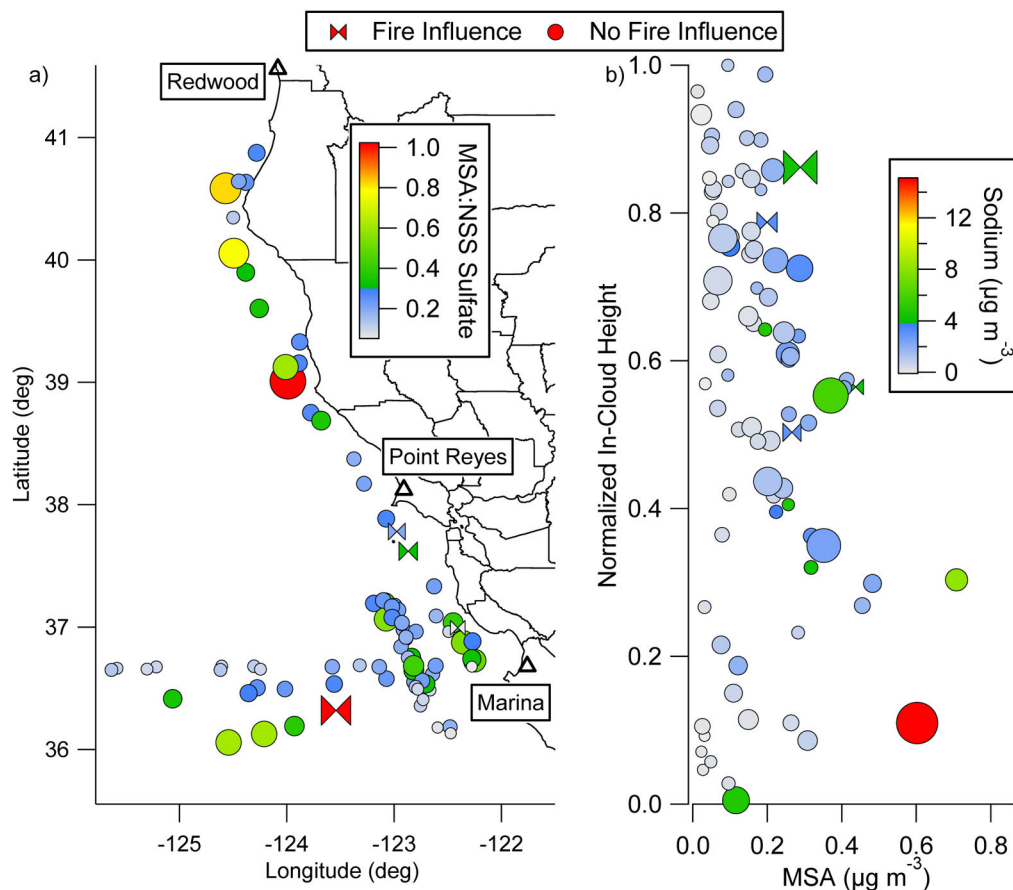


**Figure 6.**

(a) Spatial map of cloud water MSA as measured by the CIRPAS Twin Otter during the NiCE campaign between July and August 2013. Markers are sized by the MSA:nss sulfate ratio, which reach as high as 1.02. (b) Vertical in-cloud profile of MSA concentration colored by sodium, and with marker size proportional to the MSA:nss sulfate ratio. Normalized cloud height ranges from 0 (cloud base) to 1 (cloud top).

**Table 1**

Summary of correlation coefficients ( $r$ ) for the western United States and individual clusters (shown in Figure 1b) between OS mass concentrations and numerous parameters. All parameters are analyzed using their native units. Values shown are significant at 95% confidence using a two-tailed student's  $t$ -test.

	All (n=480)	C (n=60)	N (n=168)	IC (n=108)	D (n=144)
Temperature	0.60	0.60	0.71	0.75	0.70
Precipitation	-0.46	-0.61	-0.50	-0.58	-0.44
Cloud Fraction	-0.50	-0.62	-0.57	-0.57	-0.48
CWV	0.59	0.73	0.78	0.79	0.60
NDVI	--	-0.39	0.25	--	--
SO <sub>4</sub> <sup>2-</sup>	0.82	0.88	0.88	0.92	0.85
OC:EC	0.12	0.28	--	--	0.24
EC	0.28	--	0.61	0.31	--
NO <sub>3</sub> <sup>-</sup>	0.22	--	0.27	--	--
OC	0.40	--	0.48	0.55	0.32
Si	0.29	--	0.49	0.63	0.19
K	0.50	0.42	0.63	0.66	0.33
Na	0.52	0.70	0.57	0.48	0.56
V	0.44	0.43	0.82	0.58	0.46

**Table 2**

Correlation coefficients between MSA and other PM<sub>1,0</sub> species based on TACO measurements for a full year (“All”) and arranged by season (Pre-monsoon = May – June; Monsoon = July – September; Winter = November – January) in Tucson between July 2012 and June 2013. Values shown are statistically significant at 95% confidence using a two-tailed student’s t-test.

	All (n = 72)	Pre-monsoon (n = 20)	Monsoon (n = 30)	Winter (n=22)
V	0.82	0.81	0.71	-
NSS Sulfate	0.58	0.69	0.59	-
Ammonium	0.45	0.65	0.53	-
Si	0.45	0.11	0.43	-
Fe	0.33	-	-	-
Oxalate	0.29	-	-	-
Nitrate	0.26	-	0.42	-
Pb	-	-	-	-
Ni	-	-	-	-
Cu	-	-	-	0.61
Zn	-	-	-	-
K	-	-	-	-

**Table 3**

Average and maximum concentrations of MSA, oxalate (a fire tracer), and the MSA:nss sulfate ratio in various areas sampled during NiCE; Inland and Coastal areas are defined relative to the dashed line in Figure 5a.

	MSA ( $\mu\text{g m}^{-3}$ )		Oxalate ( $\mu\text{g m}^{-3}$ )		MSA:NSS $\text{SO}_4^{2-}$	
	Avg	Max	Avg	Max	Avg	Max
Inland: Background	17	68	0.02	0.11	0.03	0.11
Inland: Fire	17	57	0.20	0.40	0.02	0.09
Inland: Fresno	43	95	0.03	0.10	0.04	0.11
Inland: Cattle Feedlot	35	71	0.04	0.20	0.04	0.09
Coastal: Background	23	96	0.02	0.12	0.06	0.69
Coastal: Fire	51	106	0.22	0.73	0.09	0.14
Free Troposphere	21	189	0.03	0.62	0.07	0.92